



Review

# Molecular Orientations Change Reaction Kinetics and Mechanism: A Review on Catalytic Alcohol Oxidation in Gas Phase and Liquid Phase on Size-Controlled Pt Nanoparticles

Fudong Liu <sup>1,2,†</sup> , Hailiang Wang <sup>1,2,‡</sup>, Andras Sapi <sup>1,2,§</sup> , Hironori Tatsumi <sup>2,||</sup>,  
Danylo Zhrebetsky <sup>2</sup>, Hui-Ling Han <sup>1,2</sup>, Lindsay M. Carl <sup>1,2</sup> and Gabor A. Somorjai <sup>1,2,\*</sup>

<sup>1</sup> Department of Chemistry, University of California, Berkeley, CA 94720, USA; lfd1982@gmail.com or fudong.liu@basf.com (F.L.); hailiang.wang@yale.edu (H.W.); sapia@chem.u-szeged.hu (A.S.); lyndahan@gmail.com (H.-L.H.); lindsaymishle@gmail.com (L.M.C.)

<sup>2</sup> Materials Sciences Division, Lawrence Berkeley National Laboratory, Berkeley, CA 94720, USA; hironori\_tatsumi@shokubai.co.jp (H.T.); zhrebetsky@gmail.com (D.Z.)

\* Correspondence: somorjai@berkeley.edu; Tel.: +1-510-642-4053; Fax: +1-510-643-9668

† Current address: BASF Corporation, 25 Middlesex Essex Turnpike, Iselin, NJ 08830, USA

‡ Current address: Department of Chemistry, Yale University, 300 Heffernan Dr, West Haven, CT 06516, USA

§ Current address: Department of Applied and Environmental Chemistry, University of Szeged, Rerrich Square 1, H-6720 Szeged, Hungary

|| Current address: Nippon Shokubai Co., Ltd., 992-1 Aza-Nishioki, Okihama, Aboshi-ku, Himeji, Hyogo 671-1282, Japan

Received: 30 April 2018; Accepted: 26 May 2018; Published: 27 May 2018



**Abstract:** Catalytic oxidation of alcohols is an essential process for energy conversion, production of fine chemicals and pharmaceutical intermediates. Although it has been broadly utilized in industry, the basic understanding for catalytic alcohol oxidations at a molecular level, especially under both gas and liquid phases, is still lacking. In this paper, we systematically summarized our work on catalytic alcohol oxidation over size-controlled Pt nanoparticles. The studied alcohols included methanol, ethanol, 1-propanol, 2-propanol, and 2-butanol. The turnover rates of different alcohols on Pt nanoparticles and also the apparent activation energy in gas and liquid phase reactions were compared. The Pt nanoparticle size dependence of reaction rates and product selectivity was also carefully examined. Water showed very distinct effects for gas and liquid phase alcohol oxidations, either as an inhibitor or as a promoter depending on alcohol type and reaction phase. A deep understanding of different alcohol molecular orientations on Pt surface in gas and liquid phase reactions was established using sum-frequency generation spectroscopy analysis for in situ alcohol oxidations, as well as density functional theory calculation. This approach can not only explain the entirely different behaviors of alcohol oxidations in gas and liquid phases, but can also provide guidance for future catalyst/process design.

**Keywords:** catalytic alcohol oxidation; gas phase; liquid phase; Pt nanoparticles; sum-frequency generation spectroscopy; surface molecular orientation; density functional theory calculation

## 1. Introduction

Catalytic partial oxidation and complete oxidation of alcohols over platinum group metals (PGM) or metal oxide catalysts are fundamental processes not only in energy conversion, such as in fuel cells [1,2], but also in fine chemical synthesis and the pharmaceutical industry [3–7]. Usually, the production of aldehydes and ketones is performed through alcohol oxidation in the gas phase

at high temperatures, while the production of fine chemicals and pharmaceutical intermediates is performed in the liquid phase at low temperatures [8,9]. Many researchers have focused on the synthesis of novel, highly efficient, poisoning-resistant, or low-cost catalysts to improve productivity and selectivity, as well as to lower environmental impact [6,10–18]. However, very few studies have focused on the systematic comparison on gas phase and liquid phase alcohol oxidations over the same PGM or metal oxide catalysts at the molecular level, which is very important for the basic understanding of the reaction kinetics and mechanisms to advance and improve the catalyst and process designs for practical application.

This review paper systematically summarizes our previous work in the catalytic alcohol oxidation area, in both gas phase and liquid phase over size-controlled Pt nanoparticles [9,19–22]. The studied alcohols included C1–C4 molecules, i.e., methanol (MeOH), ethanol (EtOH), 1-propanol (1-PrOH), 2-propanol (2-PrOH), and 2-butanol (2-BuOH). Detailed comparisons of the reaction rates in both phases and the Pt nanoparticle size dependence of reaction rates, as well as product selectivity, the apparent activation energy of alcohol oxidations in both phases, and also the response to co-existing water under different reaction conditions, are all included herein. To understand the intrinsic reasons at the molecular level for differences in reaction kinetics and mechanisms in alcohol oxidation under gas and liquid phases, the sum-frequency generation (SFG) vibrational spectroscopy measurements on Pt surface under reaction conditions were conducted and discussed in detail. In aid of density functional theory (DFT) computational modeling, different alcohol molecular orientations/configurations on Pt surface in the gas phase and liquid phase reactions were confirmed, which well explained the phenomena that were observed with striking differences.

## 2. Results and Discussion

### 2.1. Turnover Rate Comparison for Alcohol Oxidation in Gas Phase and Liquid Phase

Figure 1 shows the turnover frequency (TOF) of different alcohols in catalytic oxidation reactions producing carbonyl compounds in both gas phase and liquid phase. As we can observe, different alcohols in the gas phase oxidation reaction showed distinct turnover rates; for example, at 60 °C, MeOH showed the highest TOF, followed by EtOH, 2-PrOH and 1-PrOH. The saturated vapor pressure of MeOH, EtOH, 1-PrOH and 2-PrOH at 20 and 60 °C, either cited from literature or calculated using Antoine Equation, are also shown here [23–25]. From Figure 1, it can also be seen that, interestingly, there seems to be a good correlation between gas phase alcohol oxidation reaction rates and alcohol vapor pressure. Alcohols with higher vapor pressure such as MeOH, EtOH, and 2-PrOH have many more dynamic molecules in the gas phase; thus, it can reach the catalyst surface, react to form intermediates/products, and leave the catalyst surface more efficiently. In contrast, alcohol with lower vapor pressure such as 1-PrOH has less dynamic molecules in the gas phase, and these molecules are either “reluctant” to reach the catalyst surface or “stick” to the surface upon contact without leaving quickly, thus resulting in the lower reaction rates in the gas phase oxidation reaction. For 2-BuOH oxidation in gas phase, the reaction was carried out at 80 °C; therefore, the direct comparison of reaction rates between 2-BuOH and other alcohols was not performed here.

For the liquid phase oxidation reactions using pure alcohols, in most cases, such as for MeOH, EtOH, 2-PrOH and 2-BuOH, the turnover rates were lower than those in the gas phase reaction. 1-PrOH was an exception that the liquid phase reaction rate under such condition was higher than that in the gas phase. For gas phase alcohol oxidations, it should be noted that the alcohol to oxygen ratio was controlled at 1:5 (~0.48 mM of alcohols and ~2.41 mM of O<sub>2</sub>), while in the liquid phase reaction this alcohol to oxygen ratio was much higher (~4 orders of magnitude depending on alcohol density) than that in the gas phase due to much higher density of alcohols in pure liquid phase. Therefore, for reasonable comparison, we diluted the liquid phase alcohols to one thousandth using a neutral solvent, heptane, which does not show a clear impact on the reaction kinetics of alcohol oxidations under similar reaction conditions [22]. In this way, the liquid phase alcohol concentrations ranged

from 10 to 24 mM, and the dissolved O<sub>2</sub> concentration in the liquid phase (alcohol plus heptane) was about 16.7 mM, making the liquid phase reaction conditions much more similar/comparable to the gas phase reaction conditions. It is evident that, even under comparable alcohol molecular density on Pt nanoparticle surface after 1000 times dilution including MeOH, EtOH, 1-PrOH and 2-PrOH, the reaction rates in the liquid phase were about 1~4 magnitude slower than those in the gas phase reaction. The dilution of 2-BuOH in the liquid phase was not performed, but based on the dilution results for other alcohols, the reaction rate of 2-BuOH would be further decreased upon dilution resulting in much lower activity. These results suggest that the reaction rates of catalytic alcohol oxidation heavily depended on the reaction phase (gas phase versus liquid phase), and the intrinsic root cause for such discrepancy should be understood at the molecular level.

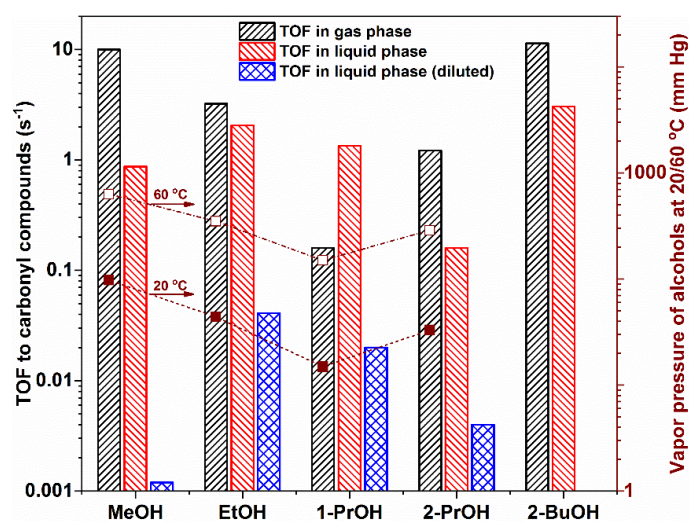


**Figure 1.** Turnover rates of alcohol oxidation to carbonyl compounds in gas and liquid phases over 6 nm Pt/MCF-17 (4.5 nm Pt/MCF-17 for 1-PrOH oxidation). Gas phase reaction: 1.33 kPa alcohol, 6.67 kPa O<sub>2</sub>, 94.66 kPa He, 60 °C reaction temperature for MeOH, EtOH, 1-PrOH, 2-PrOH and 80 °C reaction temperature for 2-BuOH. Liquid phase reaction: 15 mL alcohol, dissolved oxygen under 100 kPa for MeOH, EtOH, 1-PrOH, 2-PrOH (60 °C reaction temperature) and 300 kPa for 2-BuOH (80 °C reaction temperature). Liquid phase reaction (1000 times diluted): 15 mL heptane, 15 μL alcohol with dissolved oxygen under 100 kPa for MeOH, EtOH, 1-PrOH, 2-PrOH at 60 °C reaction temperature. The vapor pressure of MeOH, EtOH, 1-PrOH, 2-PrOH at 20 and 60 °C is also presented herein. (TOF data for MeOH, EtOH, 1-PrOH, 2-PrOH, 2-BuOH oxidations were reported in [9,19–22], respectively).

## 2.2. Size Effect of Pt Nanoparticles on Alcohol Oxidation in Gas Phase and Liquid Phase

Both gas phase and liquid phase alcohol oxidations were carried out on Pt nanoparticles with precisely controlled particle sizes, i.e., 2–9 nm Pt loaded into MCF-17 mesoporous silica. Accordingly, we could study the Pt nanoparticle size dependence of the turnover rates, as well as the product selectivity for different alcohols under both reaction conditions.

As shown in Figure 2A, for all the alcohol oxidations in the gas phase, including MeOH, EtOH, 1-PrOH, 2-PrOH at 60 °C and 2-BuOH at 80 °C, the turnover rates all showed a monotonic increase as the Pt nanoparticle size grew (except a single point for MeOH oxidation on 8 nm Pt). A very similar trend was also observed for all alcohol oxidations in the liquid phase, as shown in Figure 2B. These results indicate that the alcohol oxidation reactions preferentially took place on step sites or terrace sites on larger Pt nanoparticles, while the corner sites or edge sites on smaller Pt nanoparticle were not favorable for alcohol oxidations, probably due to their too-strong affinity to oxygenated species blocking the catalyst surface, which was not beneficial to the rate-determining dehydrogenation process of alcohol adsorbates [1,26].

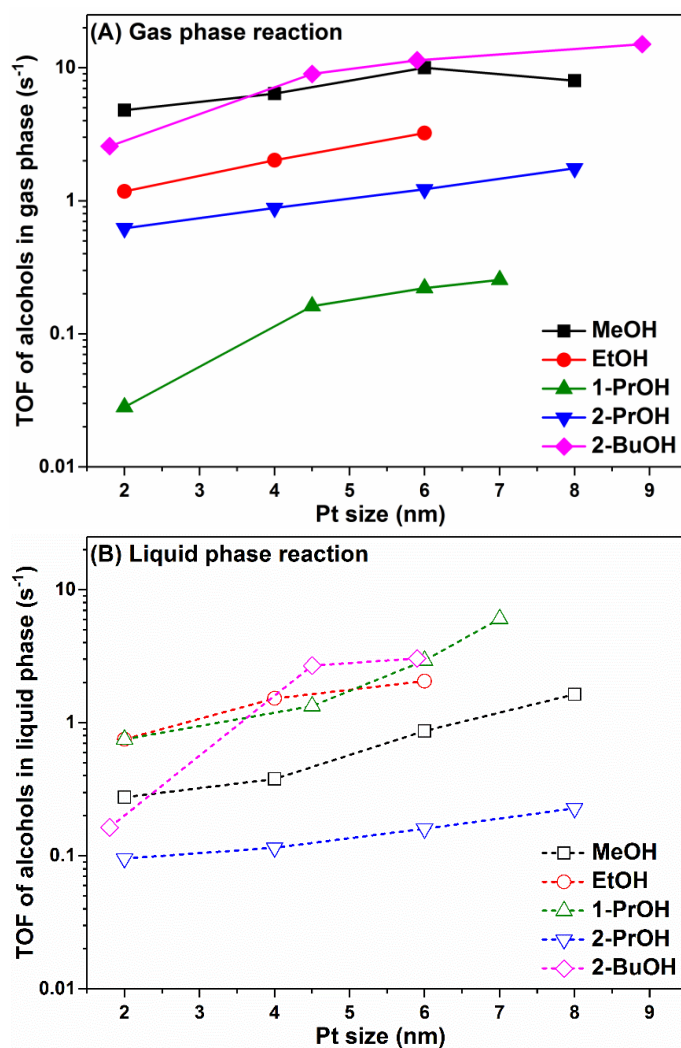


**Figure 2.** Size effect of Pt nanoparticles on TOF values of MeOH, EtOH, 1-PrOH, 2-PrOH oxidation at 60 °C and 2-BuOH oxidation at 80 °C. (A) Gas phase reaction: 1.33 kPa alcohol, 6.67 kPa O<sub>2</sub>, 94.66 kPa He; (B) Liquid phase reaction: 15 mL alcohol, dissolved oxygen under 100 kPa (300 kPa for 2-BuOH). (TOF data for MeOH, EtOH, 1-PrOH, 2-PrOH, 2-BuOH oxidations as a function of Pt nanoparticle sizes were reported in [9,19–22], respectively).

For all alcohol oxidations that we studied in both gas phase and liquid phase, except for CO<sub>2</sub> resulting from complete oxidation, the products were mainly carbonyl compounds from partial oxidation. Figure 3A shows the selectivity to carbonyl compounds in the gas phase alcohol oxidations. For gas phase MeOH oxidation, the main products were formaldehyde (less) and methyl formate (more), and the selectivity to these two compounds was about 60–70%. No clear correlation between formaldehyde plus methyl formate selectivity and Pt nanoparticle size was observed, except that the highest selectivity was observed on 4–6 nm Pt nanoparticles. For gas phase EtOH oxidation, the main product was acetaldehyde, with selectivity as high as 97%. For gas phase 1-PrOH oxidation, the main product was propanal, and similar to the MeOH case, the highest selectivity to propanal (>80%) was also observed on 4–6 nm Pt nanoparticles. For gas phase 2-PrOH oxidation, acetone was the only product. Moreover, for gas phase 2-BuOH oxidation, the selectivity to butanone on 4–6 nm Pt nanoparticles (ca. 97%) was also slightly higher than that on 2 nm Pt. Figure 3B shows the selectivity to carbonyl compounds in liquid phase alcohol oxidations. For liquid phase MeOH oxidation, interestingly, much more formaldehyde was produced than methyl formate, and the

selectivity to formaldehyde plus methyl formate (ca. 80–90%) was also much higher than that in the gas phase reaction (60–70%). Smaller Pt nanoparticles (such as 2 nm) were more likely to catalyze the deep oxidation of MeOH, thus resulting in the formation of more methyl formate, while larger Pt nanoparticles (such as 4–8 nm) were more favorable for formaldehyde formation with monotonic correlation with particle size. For all other alcohols, including EtOH, 1-PrOH, 2-PrOH and 2-BuOH, the selectivity to carbonyl compounds in the liquid phase oxidation reactions were either similar or higher than those in the gas phase reactions (see 1-PrOH data for more apparent comparison), implying that the complete oxidation of alcohols in liquid phase was actually inhibited to a certain extent, probably due to the different molecular density or molecular orientation on the Pt nanoparticle surface.

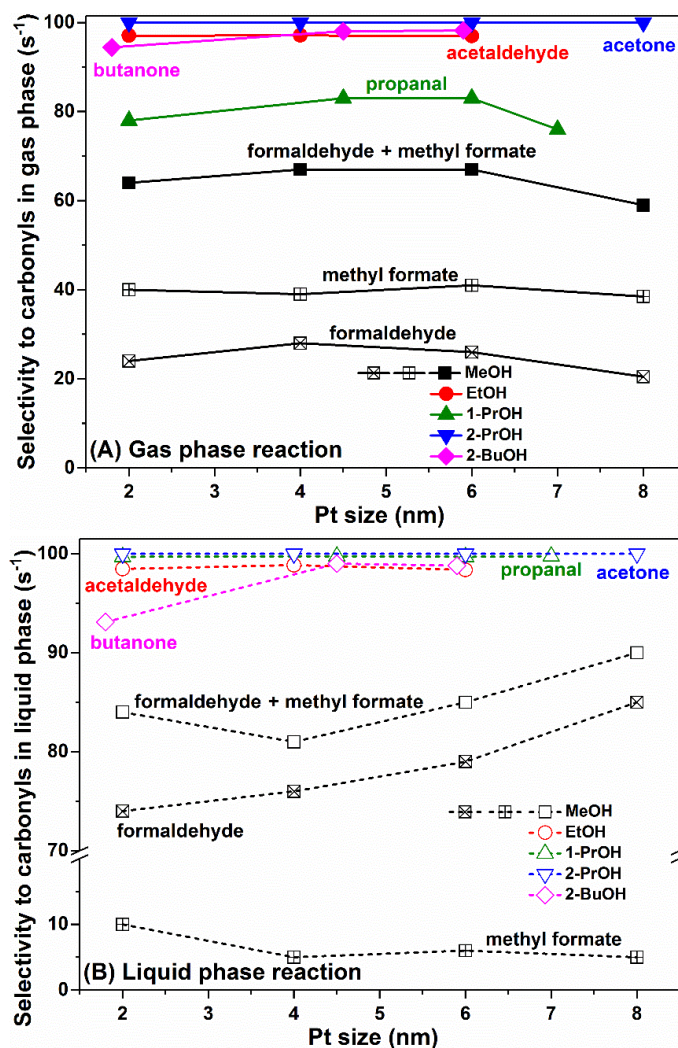


**Figure 3.** Size effect of Pt nanoparticles on product selectivity to carbonyl compounds (other than CO<sub>2</sub>) of MeOH, EtOH, 1-PrOH, 2-PrOH oxidation at 60 °C and 2-BuOH oxidation at 80 °C. (A) Gas phase reaction: 1.33 kPa alcohol, 6.67 kPa O<sub>2</sub>, 94.66 kPa He; (B) Liquid phase reaction: 15 mL alcohol, dissolved oxygen under 100 kPa for MeOH, EtOH, 1-PrOH, 2-PrOH, and 300 kPa for 2-BuOH. (Selectivity data for MeOH, EtOH, 1-PrOH, 2-PrOH, 2-BuOH oxidations as a function of Pt nanoparticle sizes were reported in [9,19–22], respectively).

### 2.3. Different Activation Energies of Alcohol Oxidation in Gas Phase and Liquid Phase on Pt Nanoparticles

To further investigate the difference of reaction kinetics for alcohol oxidations in the gas phase and liquid phase, the apparent activation energy ( $E_a$ ) on 4 nm Pt/MCF-17 for most alcohol oxidations

(4.5 nm Pt/MCF-17 for 1-PrOH oxidation) was measured and presented in Figure 4. It is very interesting to see that the apparent activation energy for all alcohol oxidations in the gas phase was much higher than that in the liquid phase, although under such reaction conditions the gas phase turnover rates were much higher than those in the liquid phase. This means that the gas phase alcohol oxidations are more sensitive to the reaction temperature, while the liquid phase alcohol oxidations do not. In practical application, if it is preferable to conduct the alcohol oxidations at higher operation temperatures, gas phase reactions are highly recommended, while if it is preferable to conduct the alcohol oxidations at lower operation temperatures, the liquid phase reactions are probably more suitable. However, the oxygen mass transfer in the liquid phase is much slower than that in the gas phase (e.g., regarding to oxygen diffusion coefficient  $D_{O_2}$ ,  $D_{O_2}$  in water, 283 K:  $1.54 \times 10^{-5}$  cm<sup>2</sup>/s,  $D_{O_2}$  in N<sub>2</sub>, 1 atm, 273 K: 0.181 cm<sup>2</sup>/s) [27,28]. It is necessary to improve the oxygen diffusion capacity in order to increase the total product yields in alcohol oxidations in the liquid phase. Besides the oxygen diffusion difference between gas phase and liquid phase reactions, the distinct alcohol molecular orientations on Pt surface in two different phases might be another important reason for activation energy discrepancy, and will be discussed in detail in the SFG spectra analysis and DFT calculation sections.

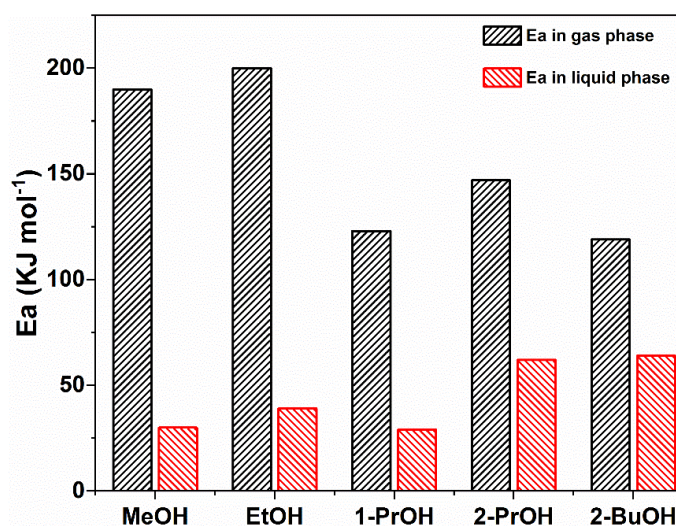


**Figure 4.** Apparent activation energy ( $E_a$ ) of alcohol oxidations in gas and liquid phases over 4 nm Pt/MCF-17 (4.5 nm Pt/MCF-17 for 1-PrOH oxidation). Gas phase reaction: 1.33 kPa alcohol, 6.67 kPa O<sub>2</sub>, 94.66 kPa He; Liquid phase reaction: 15 mL alcohol, dissolved oxygen under 100 kPa for MeOH, EtOH, 1-PrOH, 2-PrOH, and 300 kPa for 2-BuOH. ( $E_a$  data for MeOH, EtOH, 1-PrOH, 2-PrOH, 2-BuOH oxidations were reported in [9,19–22], respectively).

#### 2.4. H<sub>2</sub>O Effect on Alcohol Oxidation in Gas Phase and Liquid Phase on Pt Nanoparticles

H<sub>2</sub>O is one of the products of the complete or partial oxidation of alcohols, especially in gas phase reactions, where the selectivity to carbonyl compounds is not as high as that in the liquid phase reactions. Therefore, it is indispensable to check the H<sub>2</sub>O effect on alcohol oxidation not only in the gas phase but also in the liquid phase, which is quite essential for practical application.

As the results of relative turnover rates shown in Figure 5 demonstrate, for the gas phase MeOH, EtOH, 1-PrOH and 2-PrOH oxidations, water vapor definitely inhibited the reaction rates significantly, with the TOF values dramatically increasing upon water vapor addition. This could be simply explained by the competitive adsorption of H<sub>2</sub>O onto the Pt surface, thus obviously blocking the active sites for catalytic alcohol oxidations. However, in the case of gas phase 2-BuOH oxidation, the water vapor addition showed some promotion effect at medium H<sub>2</sub>O doping amounts (i.e., H<sub>2</sub>O content of 0.17 and 0.33), which seemed to be unusual.

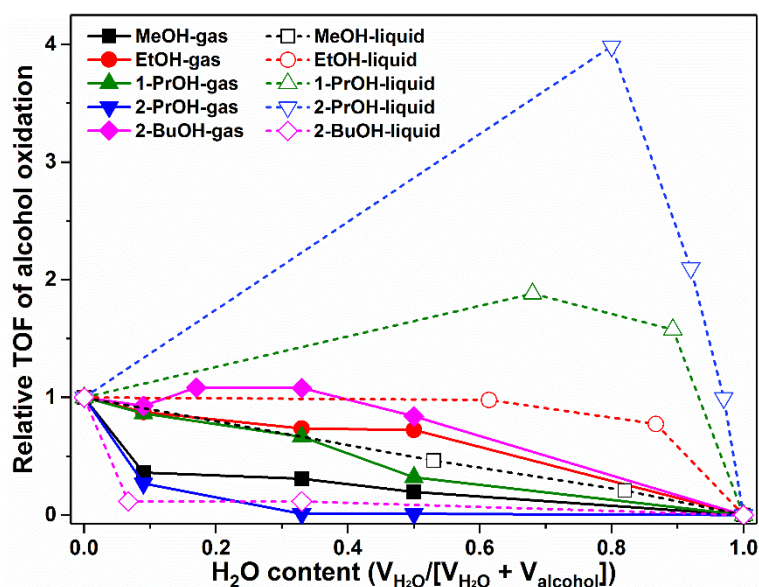


**Figure 5.** Effect of H<sub>2</sub>O addition on relative TOF of alcohol oxidations over Pt/MCF-17 in gas and liquid phases. Gas phase reaction: 1.33 kPa alcohol, 0.13–1.33 kPa water vapor, 6.67 kPa O<sub>2</sub>, He balance (in total 102.66 kPa); Liquid phase reaction: 5–10 mL alcohol, 0–10 mL distilled water, in total 15 mL volume, dissolved oxygen under 100 kPa for MeOH, EtOH, 1-PrOH, 2-PrOH and 300 kPa for 2-BuOH. Catalysts and reaction temperatures for both gas and liquid phases: 4 nm Pt/MCF-17 at 60 °C for MeOH, EtOH, 2-PrOH, 4.5 nm Pt/MCF-17 at 60 °C for 1-PrOH, and 6 nm Pt/MCF-17 at 80 °C for 2-BuOH. All data were normalized by TOF value without water addition. (H<sub>2</sub>O effect data for MeOH, EtOH, 1-PrOH, 2-PrOH, 2-BuOH oxidations were reported in [9,19–22], respectively).

In the case of the liquid phase alcohol oxidations, the responses to aqueous water addition were totally different from case to case. For example, with regard to liquid MeOH oxidation, H<sub>2</sub>O showed a nearly linear inhibition effect on reaction rate, but still the inhibition effect was not as strong as that in the gas phase reaction. In the case of the liquid phase EtOH oxidation, the inhibition effect of H<sub>2</sub>O seemed to be mitigated to a certain extent. While, for the liquid phase 1-PrOH and 2-PrOH oxidations, H<sub>2</sub>O actually acted as a “promoter” or “co-catalyst”, which significantly increased the turnover rates. Such striking difference of reaction rates in response to aqueous water in the liquid phase alcohol oxidations comparing to response to water vapor in the gas phase alcohol oxidations was mainly due to the totally different alcohol molecular density and/or alcohol molecular orientation on the Pt surface. As for the liquid phase 2-BuOH oxidation, the impact of aqueous water on reaction rate was totally opposite to other alcohols. Even with a very small amount of aqueous water addition, such as an H<sub>2</sub>O content of 0.07, the turnover rate dramatically decreased to ca. 12% of the initial value, indicating that aqueous water here actually acted as a “poisoning agent” for the liquid phase 2-BuOH oxidation.

So far, totally opposite effects were observed for H<sub>2</sub>O on gas phase and liquid phase 2-BuOH oxidations, in contrast to other alcohols, which can probably be explained by the hydrophilicity difference of alcohols. MeOH, EtOH, 1-PrOH and 2-PrOH are all miscible in water, while 2-BuOH has a solubility of only 12.5 g per 100 mL of H<sub>2</sub>O due to the existence of more hydrophobic alkyl chains [9,29]. The capping agent that we used for Pt nanoparticle synthesis, which was polyvinylpyrrolidone (PVP), actually showed amphiphilicity. In the case of the gas phase 2-BuOH oxidation with relatively high mobility of alcohol and H<sub>2</sub>O molecules, once the 2-BuOH molecules had reached and attached to the Pt surface, H<sub>2</sub>O could not be adsorbed onto the surface anymore in any significant amount due to the hydrophobic nature of the 2-BuOH molecules. Therefore, water vapor only showed a slight inhibition effect, or even some promotion effect (probably due to

the more hydroxyl group formation in the presence of H<sub>2</sub>O) [30,31], on gas phase 2-BuOH oxidation. Contrastingly, in the case of the liquid phase 2-BuOH oxidation with relatively low mobility of alcohol and H<sub>2</sub>O molecules, aqueous water would preferably gather around the Pt surface due to the hydrophobic nature of 2-BuOH. Such aqueous water layer blocked the access to the surface active sites thus resulting in the decrease of turnover rate in the liquid 2-BuOH oxidation [9].

### 2.5. Case Study of 1-PrOH Oxidation Using SFG Spectra Analysis on Pt Thin Film and DFT Calculation in Gas and Liquid Phases

To fully understand the picture of how alcohol molecules interact with the Pt surface under different reaction conditions, taking 1-PrOH as first example, we conducted SFG spectra study at 60 °C, which is an in situ technique with surface-specific characteristics, on Pt thin films prepared by electron-beam deposition. Figure 6 shows the SFG spectra of 1-PrOH in gas phase on Pt thin film during reaction at 60 °C with 101.33 kPa of O<sub>2</sub> and different partial pressures of gas phase 1-PrOH, as well as the SFG spectra of 1-PrOH on Pt thin films at 60 °C purged by N<sub>2</sub> in the gas phase and liquid phase. As can clearly be seen from Figure 6a,b, the SFG peaks that can be assigned to symmetric CH<sub>2</sub> stretching mode at ca. 2840 cm<sup>-1</sup>, symmetric CH<sub>3</sub> stretching mode at ca. 2870 cm<sup>-1</sup>, asymmetric CH<sub>2</sub> stretching mode at ca. 2910 cm<sup>-1</sup>, CH<sub>3</sub> Fermi resonance at ca. 2935 cm<sup>-1</sup>, and asymmetric CH<sub>3</sub> stretching mode at ca. 2970 cm<sup>-1</sup> can be observed on the Pt surface under 1.87 and 9.07 kPa of 1-PrOH with O<sub>2</sub>. However, these spectra showed noticeable differences not only in the strength of CH<sub>2</sub> peaks but also in the ratios between asymmetric and symmetric methyl stretches. This is absolutely clear evidence that surface 1-PrOH molecule orientation on Pt is highly dependent on the alcohol molecular density in the gas phase. It should be noted that our SFG spectra were measured under *ppp* polarization. Therefore, the absolute 1-PrOH molecule orientation cannot be directly determined. However, SFG theory predicts that a change in the orientation of specific functional groups (such as -CH<sub>3</sub> groups in this study) relative to the studied surface can result in the intensity ratio change of different vibration modes [22]. In such studies, the surface of Pt was considered to possess C<sub>∞v</sub> symmetry, while the 1-PrOH molecule orientation on the Pt surface was assumed to be isotropic with regard to the azimuthal angle to the z-axis. Therefore, the average tilt angle of -CH<sub>3</sub> group from the Pt surface ( $\theta$ ) could be described by such a measurement, and changes in the asymmetric/symmetric mode ratio among the spectra were accordingly representative of a change of  $\theta$  [21]. A low value of  $\theta$  describes a molecule with its methyl group pointing up from the surface ("standing up" configuration), and a high value describes a molecule close to the surface ("lying down" configuration) [22]. The ratio of asymmetric/symmetric stretches of -CH<sub>3</sub> group under 1.87 kPa of 1-PrOH with O<sub>2</sub> was ca. 0.5:1, while this ratio significantly increased to 2:1 under 9.07 kPa of 1-PrOH with O<sub>2</sub>, which was four times higher. This indicates a significant change in  $\theta$  between low and high 1-PrOH partial pressure, and thus a different molecular orientation on the Pt surface.

Furthermore, as shown in Figure 6c,d, we also measured the SFG spectra of 1-PrOH on the Pt surface under N<sub>2</sub> purge with 10.67 kPa partial pressure in the gas phase and pure 1-PrOH in the liquid phase. The SFG spectrum recorded for gas phase 1-PrOH under such conditions showed peaks that could be assigned to -CH<sub>3</sub> groups with symmetric stretching mode at ca. 2870 cm<sup>-1</sup>, strong Fermi resonance at ca. 2935 cm<sup>-1</sup>, and asymmetric stretching mode at ca. 2960 cm<sup>-1</sup>, as well as -CH<sub>2</sub> groups as weak shoulders with symmetric stretching mode at ca. 2840 cm<sup>-1</sup> and asymmetric stretching mode at ca. 2910 cm<sup>-1</sup>. This spectrum was pretty similar to the one recorded under O<sub>2</sub> with 1-PrOH with a relatively larger partial pressure in Figure 6b, although in this case, both the asymmetric and symmetric stretches from -CH<sub>3</sub> and -CH<sub>2</sub> groups showed some increase in peak intensity, mainly due to the higher 1-PrOH density on Pt surface. Contrastingly, the SFG spectrum recorded for liquid phase 1-PrOH showed significantly changed peak patterns compared to the gas phase, with slightly decreased peak intensity in -CH<sub>2</sub> stretching modes and greatly increased intensity ratio between asymmetric and symmetric stretching modes from -CH<sub>3</sub>. We believe that the average tilt angle of -CH<sub>3</sub> group from Pt surface,  $\theta$ , for 1-PrOH in the liquid phase became much smaller than that in



the gas phase, which means that the molecular structure in the liquid phase was more ordered and more preferentially in a “standing up” configuration than the “lying down” configuration in the gas phase [21].

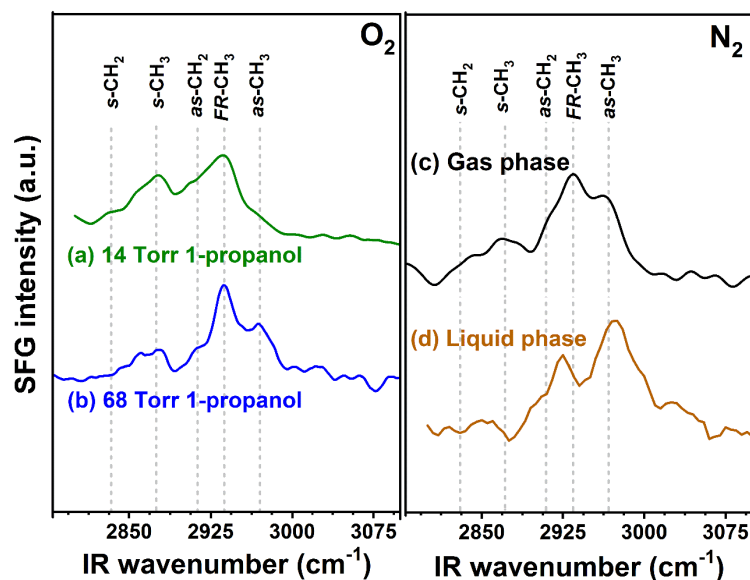


**Figure 6.** SFG spectra collected for gas phase 1-PrOH on Pt thin film during reactions at 60 °C with 101.33 kPa of O<sub>2</sub>: (a) 1.87 kPa (14 Torr) of 1-PrOH; (b) 9.07 kPa (68 Torr) of 1-PrOH. SFG spectra collected for 1-PrOH on Pt thin film at 60 °C purged with N<sub>2</sub>: (c) gas phase, 10.67 kPa of 1-PrOH; (d) liquid phase 1-PrOH. (SFG data for 1-PrOH oxidation were reported in [21]. Reproduced with permission from [21]. Copyright 2018 American Chemical Society.).

To better understand the molecular orientation of 1-PrOH on Pt surface in gas and liquid phases, we performed DFT theoretical calculation to simulate the concentration-dependent 1-PrOH configurations on Pt(111), which is the dominant surface for Pt nanoparticles used for alcohol oxidation reactions. More details about DFT calculation, as well as comprehensive results, can be found in our previous publication [21], while Figure 7 herein shows the minimum energy configurations of 1-PrOH molecules on Pt(111) surface with a surface molecular coverage of 0.94 molecules/nm<sup>2</sup>, which represents the gas phase condition, as well as a surface molecular coverage of 3.75 molecules/nm<sup>2</sup>, which represents the liquid phase condition. As we can see, under the gas phase condition, the 1-PrOH molecules were nearly “lying down” on the Pt surface, with the bisectrix connecting hydroxyl-O and methyl-C forming 6° angle relative to the surface (as shown in Table 1). Under the liquid phase condition, the 1-PrOH molecules were nearly “standing up” on the Pt surface with the bisectrix forming 41° angle relative to the surface (as shown in Table 1). These results are very consistent with the SFG spectral data and well explain the relative peak intensity changes that we observed for 1-PrOH on Pt thin film in the gas phase versus liquid phase. It should also be noted that, as shown in Table 1, the distance between the hydrogen atoms from alcohol hydroxyl group in 1-PrOH and Pt surface under the liquid phase condition was calculated as 0.261 nm, which was 0.056 nm closer to the Pt surface than the corresponding distance under the gas phase condition, i.e., 0.317 nm. This indicates that the hydroxyl group, and possibly also the α-H connecting to the same carbon atom in the 1-PrOH molecule, were much more easily activated/dehydrogenated in the liquid phase than in the gas phase, well explaining why the activation energy for 1-PrOH oxidation in the liquid phase was much lower than that in the gas phase.

**Table 1.** 1-Propanol molecule orientation as angle of C–C bonds relative to surface normal, and nearest surface–molecule distance for different concentrations of molecules on Pt(111) surface [21].

Concentration (molecules/nm <sup>2</sup> )	$\alpha$ (°)	H <sub>alc</sub> -Pt (nm)
0.94	6	0.317
3.75	41	0.261

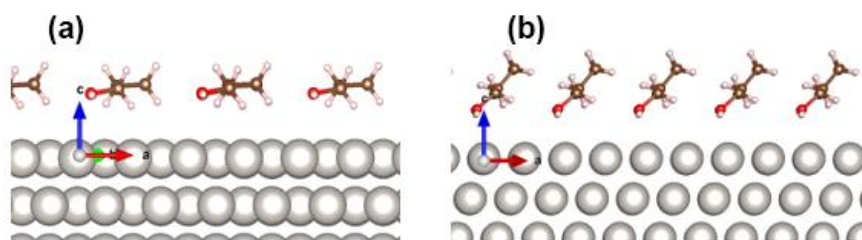


**Figure 7.** Minimum energy configurations of 1-PrOH molecules on Pt(111) surface for (a) gas phase (0.94 molecules/nm<sup>2</sup>) and (b) liquid phase (3.75 molecules/nm<sup>2</sup>) from DFT calculation (Pt—gray, C—brown, O—red, H—pink). (DFT results for 1-PrOH oxidation were reported in [21]. Reprinted with permission from [21]. Copyright 2018 American Chemical Society.).

### 2.6. Case Study of 2-PrOH Oxidation Using SFG Spectra Analysis on Pt Nanoparticles and DFT Calculation in Gas Liquid Phases

Similar to the 1-PrOH case, we also performed SFG spectra analysis of 2-PrOH oxidation in both gas phase and liquid phase on 4 nm Pt nanoparticles, which was more representatively reflective of the real catalytic reactions that we studied. As shown in Figure 8a, in the gas phase 2-PrOH oxidation reaction, three noticeable SFG peaks showed up, which could be ascribed to symmetric stretches of CH<sub>3,ss</sub> at ca. 2875 cm<sup>-1</sup>, Fermi resonance mode of CH<sub>3,fr</sub> at ca. 2940 cm<sup>-1</sup>, and asymmetric stretches of CH<sub>3,as</sub> at ca. 2970 cm<sup>-1</sup>. The intensity ratio between asymmetric and symmetric stretches of –CH<sub>3</sub> was relatively small in this case. Not surprisingly, as shown in Figure 8b, in the liquid phase 2-PrOH oxidation reaction, all three SFG peaks ascribed to CH<sub>3,ss</sub>, CH<sub>3,fr</sub>, CH<sub>3,as</sub> showed up, along with a stretching peak from –CH group at ca. 2905 cm<sup>-1</sup>; however, the intensity ratio between asymmetric and symmetric stretches of –CH<sub>3</sub> showed significant increase compared to the gas phase spectrum. These results indicate that the average tilt angle of –CH<sub>3</sub> group from Pt nanoparticle surface,  $\theta$ , must have changed from a high value in the gas phase to a low value in the liquid phase, suggesting a change in the 2-PrOH molecular configurations from “lying down” to “standing up” on Pt surface, respectively. More detailed discussions about the possibility of 2-PrOH orientation varieties in different phases determined by SFG experimental data can be found in our previous publication [22].

To further confirm the 2-PrOH molecular configuration on the Pt surface, similarly to the 1-PrOH case, DFT theoretical calculation was also performed in our study. As the nanoparticles and nanoparticle-molecule complexes were too large for ab initio calculation, we still used the most dominant Pt(111) surface to investigate the concentration/phase dependence of 2-PrOH molecular orientations. As shown in Figure 9a, the minimum energy configuration of 2-PrOH molecules on Pt(111) surface with a low surface coverage of 0.94 molecules/nm<sup>2</sup>, which is representative of the gas phase condition, showed a “lying down” pattern, with both of the C–C bonds forming 86° relative to the surface normal (Table 2). In contrast, as shown in Figure 9b, the minimum energy configuration of 2-PrOH molecules on the Pt(111) surface with high surface coverage of 3.75 molecules/nm<sup>2</sup>, which is representative of the liquid phase condition, showed a “standing up” pattern with one C–C bond forming 84° and the other forming 38° relative to the surface normal (Table 2). The steric molecular interaction effect can easily explain this phenomenon, i.e., alcohol molecules are forced to take the “standing up” position in order to pack more molecules on the Pt surface [22]. As shown in Table 2, the 2-PrOH molecular orientation change from “lying down” to “standing up” on the Pt surface also

resulted in the distance change between  $\alpha$ -H and the nearest Pt atom, i.e., 0.445 nm in the gas phase and 0.257 nm in the liquid phase. Obviously, in such cases, much easier cleavage/dehydrogenation of  $\alpha$ -H from  $\alpha$ -C (which was considered as the rate-determining step in 2-PrOH oxidation [1]) can be achieved in the liquid phase than in the gas phase. This is also consistent with the observation that 2-PrOH oxidation showed much lower activation energy in the liquid phase than that in the gas phase [22].

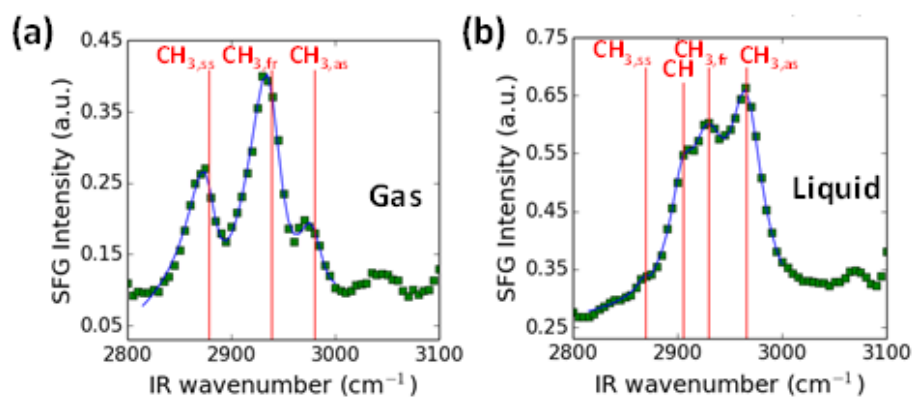


**Figure 8.** SFG spectra obtained on the surface of 4 nm Pt nanoparticles for 2-PrOH oxidation under (a) gas phase and (b) liquid phase reaction conditions. (SFG data for 2-PrOH oxidation were reported in [22]. Reprinted with permission from [22]. Copyright 2014 American Chemical Society.)

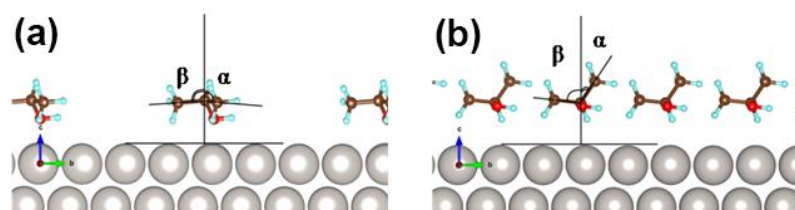


**Figure 9.** Minimum energy configurations of 2-PrOH molecules on Pt(111) surface for (a) gas phase (0.94 molecules/nm<sup>2</sup>) and (b) liquid phase (3.75 molecules/nm<sup>2</sup>) from DFT calculation (Pt—gray, C—brown, O—red, H—blue). (DFT results for 2-PrOH oxidation were reported in [22]. Reprinted with permission from [22]. Copyright 2014 American Chemical Society.)

**Table 2.** 2-Propanol molecular orientations as angles of C—C bonds relative to surface normal, and nearest  $\alpha$ -H—Pt distances for different concentrations of 2-propanol molecules on Pt(111) surface [22].

Concentration (molecules/nm <sup>2</sup> )	$\alpha$ (°)	$\beta$ (°)	$\alpha$ -H—Pt (nm)
0.94	86	86	0.445
3.75	38	84	0.257

### 2.7. Case Study of 2-BuOH Oxidation Using SFG Spectra Analysis on Pt Thin Film in Gas Phase: O<sub>2</sub> and H<sub>2</sub>O Effect

To better understand the 2-BuOH oxidation reaction in the gas phase, we performed SFG spectra analysis using various oxygen concentrations as well as added water vapor to see if there was any influence on the 2-BuOH molecular orientation. As shown in Figure 10a, we first collected the SFG spectrum under 2-BuOH with N<sub>2</sub>, and the peaks ascribed to —CH<sub>3</sub> symmetric stretching mode at ca. 2880 cm<sup>-1</sup>, —CH<sub>3</sub> Fermi resonance mode at ca. 2945 cm<sup>-1</sup>, and —CH<sub>3</sub> asymmetric stretching mode at ca. 2975 cm<sup>-1</sup> could be observed. Based on the SFG results for 1-PrOH, 2-PrOH on the Pt surface, and judging from the intensity ratio between asymmetric and symmetric stretching mode for 2-BuOH

case, it can be empirically deduced that the 2-BuOH molecules also had a “lying down” configuration on the Pt surface in the gas phase. Interestingly, in the presence of oxygen, even at a relatively low level ( $O_2$ :2-BuOH = 3:1), a much higher SFG signal for 2-BuOH was observed than that in the presence of inert  $N_2$ . Further increasing the oxygen content to  $O_2$ :2-BuOH = 10:1 yielded an even higher SFG signal. These results indicate that with the co-existence of  $O_2$  in the gas phase, either the 2-BuOH molecules on Pt surface tended to be more ordered, or much higher surface 2-BuOH molecular density could be achieved.

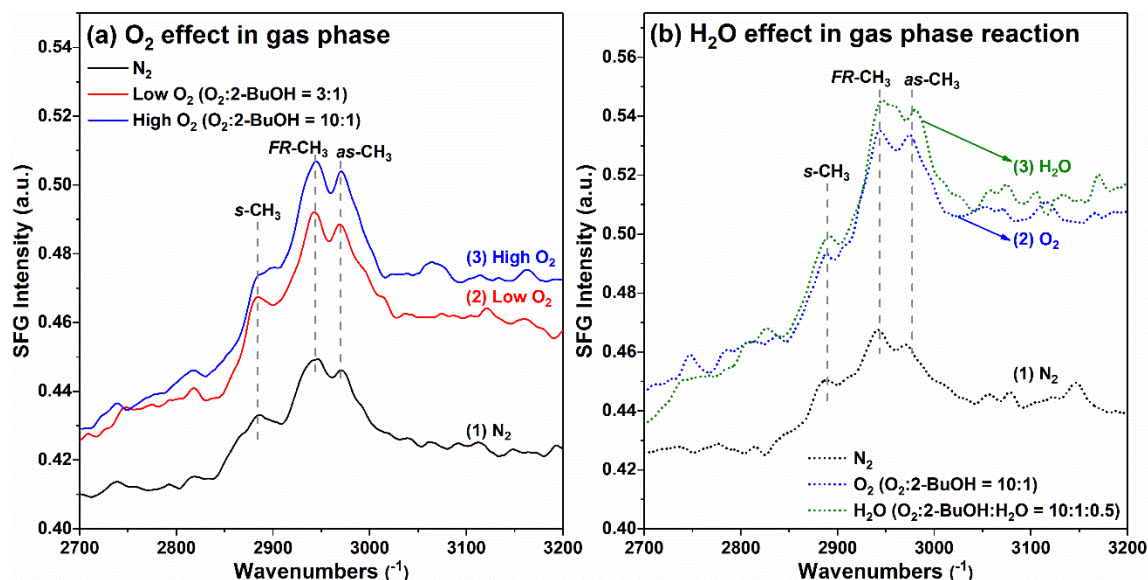


**Figure 10.** SFG spectra of gas phase 2-BuOH on Pt thin film at 80 °C (a) with varying ratios of oxygen to alcohol (i.e.,  $N_2$  only, low  $O_2$  content with  $O_2$ :2-BuOH = 3:1, and high  $O_2$  content with  $O_2$ :2-BuOH = 10:1), and (b) in the presence of water vapor (i.e.,  $N_2$  only, high  $O_2$  content with  $O_2$ :2-BuOH = 10:1, and in the presence of  $H_2O$  with  $O_2$ :2-BuOH: $H_2O$  = 10:1:0.5).

In order to provide insight into the influence of water vapor on 2-BuOH oxidation on Pt surface in the gas phase, the SFG spectra were also taken under reaction conditions with and without  $H_2O$  addition. As the results shown in Figure 10b indicate, again, the introduction of  $O_2$  into system resulted in the sharp increase of SFG peak intensity, but the introduction of water vapor into system seemed to have little effect on the SFG peaks (even with some increased peak intensity for  $-CH_{3,fr}$  and  $-CH_{3,as}$ ). These results well support the catalytic data for the gas-phase 2-BuOH oxidation, in which the addition of water vapor had minimal effect on the reaction turnover rates. The SFG spectra analysis for 2-BuOH oxidation on Pt surface in the liquid phase is essential and highly recommended in future study to provide more information for alcohol oxidation chemistry in both phases at molecular level.

### 3. Materials and Methods

#### 3.1. Pt Nanoparticle Synthesis and Encapsulation into Mesoporous Silica MCF-17

The Pt nanoparticles with sizes ranging from 2 to 9 nm were synthesized by a polyvinylpyrrolidone (PVP) assisted polyol process using ethylene glycol as reducing agent. The detailed procedures have been reported in our previous study [9,19–22]. Transmission electron microscopic (TEM) images showed that the as-synthesized Pt nanoparticles had narrow particle size distributions, and the high resolution TEM images with legible lattice fringes indicated that Pt(111) was the most favorable exposed surface.

Mesoporous silica MCF-17 with 20–30 nm pore size was used as support to immobilize the Pt nanoparticles. The as-synthesized Pt nanoparticles and MCF-17 support were mixed in ethanol solvent followed by sonication with 40 kHz, 80 W for 2 h. The MCF-17 supported Pt nanoparticles

were collected by centrifugation followed by washing with ethanol for three times and drying at 80 °C overnight. Inductively coupled plasma atomic emission spectroscopy (ICP-AES) was used to determine the amount of Pt nanoparticles encapsulated in MCF-17. A known amount of Pt/MCF-17 catalysts were sonicated in ethanol first for good dispersion and then drop-casted on silica wafers followed by drying at room temperature for gas phase reactions. A known amount of Pt/MCF-17 catalysts were used, as it was for liquid phase reactions. The calculation of the active site number was based on the ICP-AES results and the size of the particles for turnover rates (TOF) calculation, assuming that Pt(111) surface was favorably exposed and every surface Pt atom was active in the catalytic alcohol oxidation reactions. The way of molecule adsorption on Pt surface, the influence of organic PVP capping agents and also the interface between Pt nanoparticle and mesoporous SiO<sub>2</sub> support was not taken into account for TOF calculation.

### 3.2. Catalytic Oxidation of Alcohols over Pt/MCF-17 Catalysts in Gas Phase and Liquid Phase

The gas phase alcohol oxidation reactions were performed in a gold-covered batch reactor, and the temperature of Pt/MCF-17 catalysts was precisely controlled by a boron nitride heater plate. Usually, in the typical gas phase reactions, 1.33 kPa of alcohols, 6.67 kPa of O<sub>2</sub> and 94.66 kPa of He were used, and the gas was circulated with a metal bellow pump. A gas chromatograph (GC) integrated with a flame ionization detector (FID) was used to monitor the gas composition online. All the alcohol conversions were kept under 10% during the data collection to calculate the turnover rates (TOF). For water effect study in the gas phase, 0.13–1.33 kPa of water vapor was introduced to the reaction chamber keeping the total pressure still as 102.66 kPa.

The liquid phase alcohol oxidation reactions were carried out in a Teflon-lined stainless-steel autoclave (Parr reactor, total volume of 100 mL). Usually, 15 mg catalysts were well dispersed in 15 mL liquid alcohols. The headspace of the reactor (85 mL) was purged and pressurized with O<sub>2</sub> (100 kPa for MeOH, EtOH, 1-PrOH, 2-PrOH, and 300 kPa for 2-BuOH) before the reaction started. The system was then heated to an elevated temperature and kept there for 3 h under continuous stirring. After the reaction, the mixture was cooled down, and the headspace gas was leaked to the GC-FID through an evacuated gas chamber for the gas phase product analysis. After the disassembly of the autoclave reactor, the catalyst was separated with centrifugation and the liquid phase was analyzed with GC-FID to obtain the liquid phase product information. For water effect study in the liquid phase, the ratio of H<sub>2</sub>O in alcohols was adjusted to 0–75 V<sub>H<sub>2</sub>O</sub>/V<sub>total</sub> % while the total amount of liquid was kept at 15 mL. For low-concentration alcohol oxidation in the liquid phase, heptane was used as a diluter, and the ratio of alcohols to heptane was controlled at 1:1000.

### 3.3. SFG Spectral Analysis for 1-PrOH, 2-PrOH and 2-BuOH Oxidation in Gas and Liquid Phases

The SFG spectra taken for in situ catalytic 1-PrOH and 2-BuOH oxidations were carried out on Pt thin film prepared by electron beam deposition method [21]. The SFG spectra taken for in situ catalytic 2-PrOH oxidations were carried out on silica embedded 4 nm Pt nanoparticles deposited by deposition of Langmuir-Blodgett films onto sapphire prisms followed by calcination in air at 550 °C for 3 h [22]. All the SFG experiments were carried out in a system described in our previous work [32]. An active/passive mode-locked Nd:YAG laser (Continuum Leopard D10, 20 ps, 20 Hz, 1064 nm) was used to pump frequency conversion stages to generate two pulses, a visible pulse (532 nm, 130 μJ) and a tunable mid-IR pulse (2800 to 3600 cm<sup>-1</sup>, 200 μJ). These pulses were overlapped at 62° (visible) and 45° (mid-IR) on the sample which had been deposited on the bottom of a quartz prism. Experiments were performed in the *ppp* polarization combination. The SFG signal was collected using a photomultiplier tube (PMT) accompanied by a gated integrator to improve the signal quality. The SFG spectra presented in this study had a resolution of 4 cm<sup>-1</sup>, and each spectrum involved the average of at least 100 or 200 samplings to increase the signal-to-noise ratio for spectral analysis. Using a home-built cell, the surface was heated, and a recirculating mixture of the reaction gases/liquid

was passed onto the Pt film/Pt nanoparticles. All the SFG spectra were normalized with the reference spectrum taken with a z-cut quartz.

#### 3.4. DFT Calculation of Molecular Orientation of 1-PrOH and 2-PrOH on Pt Surface in Gas Phase and Liquid Phase

All geometry optimizations within the frame of DFT were performed with first-principles periodic system calculations using VASP software package [33]. The projector augmented wave (PAW) method was utilized to construct the basis set for the one-electron wave functions with plane-wave basis set limited by the cutoff energy of 400 eV [34]. For the constructed slabs, at least  $3 \times 3 \times 1$  (for 1-PrOH) or  $5 \times 5 \times 1$  (for 2-PrOH) Monkhorst-Pack k-point grid was used (depending on the geometrical dimensions). The Pt(111) slabs used were four layers thick and contained a minimum 1.7 nm (for 1-PrOH) or 1.2 nm (for 2-PrOH) vacuum space to exclude surface-surface interaction. The electronic steps were carried out with the energy convergence of  $10^{-5}$  eV while the force convergence of ionic steps was set to be  $5 \times 10^{-2}$  eV/nm. For 1-PrOH, geometry optimization was performed using the PBE functional including Van der Waals interaction in DF approximation [35,36]. For 2-PrOH, geometry optimization was performed using the Perdew-Wang functional in generalized gradient approximation (GGA) [37]. The selected two constructed systems corresponded to two different concentrations of 1-PrOH and 2-PrOH molecules on Pt surface. At a low surface molecular coverage of 0.94 molecules/nm<sup>2</sup>, the next-nearest distance between atoms of different molecules was more than 0.8 nm. At this separation distance, the alcohol molecules were considered to have minimal interaction at DFT level of theory. Therefore, we assumed that the corresponding molecular configuration represented the adsorption of alcohols from the low-pressure gas phase. On the other hand, the determined concentration of the 1-PrOH and 2-PrOH molecules in the liquid phase was about 3.94 molecules/nm<sup>2</sup>, which was very close to the higher modeled surface concentration of 3.75 molecules/nm<sup>2</sup> that we could call liquid phase condition.

#### 4. Conclusions

C1-C4 alcohol oxidation reactions including MeOH, EtOH, 1-PrOH, 2-PrOH and 2-BuOH in the gas phase and liquid phase over size-controlled Pt nanoparticles were systematically studied herein. The catalytic oxidation of alcohols in the gas phase showed much higher turnover rates than those in the liquid phase under the comparable surface density of reactants. Larger Pt nanoparticles exhibited higher turnover rates for both gas phase and liquid phase reactions, and in general, the liquid phase reaction showed very similar or higher selectivity to carbonyl compounds due to less complete oxidation reaction occurring forming CO<sub>2</sub> than the gas phase reaction. Interestingly, much lower apparent activation energy was observed for the alcohol oxidations in the liquid phase than those in the gas phase. In most cases, co-existing H<sub>2</sub>O acted as a promoter for the liquid phase alcohol oxidations (especially for 1-PrOH and 2-PrOH) and as an inhibitor for the gas phase alcohol oxidations; however, totally the opposite H<sub>2</sub>O effect was observed for 2-BuOH oxidation compared to other studied alcohols, which can be explained by hydrophilicity/hydrophobicity change for longer carbon chain alcohols. SFG spectra analysis suggested that significant change of molecular orientations was present for 1-PrOH and 2-PrOH on the Pt surface in the gas phase and liquid phase, and DFT calculation results confirmed that the alcohol molecules were mainly “lying down” on the Pt surface in the gas phase and “standing up” on Pt surface in the liquid phase. This led to totally distinct reaction kinetics and mechanisms for alcohol oxidations in different phases. SFG spectra analysis also revealed that the presence of O<sub>2</sub> could result in more ordered surface species or higher density of alcohol molecules on Pt surface in the gas phase 2-BuOH oxidation, and H<sub>2</sub>O did not show an obvious influence on surface 2-BuOH molecules, explaining well why H<sub>2</sub>O had little impact on turnover rates in the gas phase reaction. More systematic SFG spectra analysis and DFT calculation for the liquid phase 2-BuOH oxidation on Pt surface are necessary in future study.

**Acknowledgments:** This work was supported by the Director, Office of Basic Energy Sciences, Materials Science and Engineering Division of the U.S. Department of Energy under Contract No. DE-AC02-05CH11231.

**Conflicts of Interest:** The authors declare no conflict of interest.

## References

1. DiCosimo, R.; Whitesides, G.M. Oxidation of 2-propanol to acetone by dioxygen on a platinumized electrode under open-circuit conditions. *J. Phys. Chem.* **1989**, *93*, 768–775. [[CrossRef](#)]
2. Zhao, X.; Yin, M.; Ma, L.; Liang, L.; Liu, C.; Liao, J.; Lu, T.; Xing, W. Recent advances in catalysts for direct methanol fuel cells. *Energy Environ. Sci.* **2011**, *4*, 2736–2753. [[CrossRef](#)]
3. Besson, M.; Gallezot, P. Selective oxidation of alcohols and aldehydes on metal catalysts. *Catal. Today* **2000**, *57*, 127–141. [[CrossRef](#)]
4. Gauthier, E.; Benziger, J.B. Gas management and multiphase flow in direct alcohol fuel cells. *Electrochim. Acta* **2014**, *128*, 238–247. [[CrossRef](#)]
5. Gomes, J.F.; Bergamaski, K.; Pinto, M.F.S.; Miranda, P.B. Reaction intermediates of ethanol electro-oxidation on platinum investigated by sfg spectroscopy. *J. Catal.* **2013**, *302*, 67–82. [[CrossRef](#)]
6. Mallat, T.; Baiker, A. Oxidation of alcohols with molecular oxygen on solid catalysts. *Chem. Rev.* **2004**, *104*, 3037–3058. [[CrossRef](#)] [[PubMed](#)]
7. Jelemensky, L.; Kuster, B.F.M.; Marin, G.B. Multiple steady-states for the oxidation of aqueous ethanol with oxygen on a carbon supported platinum catalyst. *Catal. Lett.* **1994**, *30*, 269–277. [[CrossRef](#)]
8. Ciriminna, R.; Pandarus, V.; Béland, F.; Xu, Y.-J.; Pagliaro, M. Heterogeneously catalyzed alcohol oxidation for the fine chemical industry. *Org. Process Res. Dev.* **2015**, *19*, 1554–1558. [[CrossRef](#)]
9. Tatsumi, H.; Liu, F.; Han, H.-L.; Carl, L.M.; Sapi, A.; Somorjai, G.A. Alcohol oxidation at platinum–gas and platinum–liquid interfaces: The effect of platinum nanoparticle size, water coadsorption, and alcohol concentration. *J. Phys. Chem. C* **2017**, *121*, 7365–7371. [[CrossRef](#)]
10. Davis, S.E.; Ide, M.S.; Davis, R.J. Selective oxidation of alcohols and aldehydes over supported metal nanoparticles. *Green Chem.* **2013**, *15*, 17–45. [[CrossRef](#)]
11. Feng, J.; Ma, C.; Miedziak, P.J.; Edwards, J.K.; Brett, G.L.; Li, D.; Du, Y.; Morgan, D.J.; Hutchings, G.J. Au-pd nanoalloys supported on mg-al mixed metal oxides as a multifunctional catalyst for solvent-free oxidation of benzyl alcohol. *Dalton Trans.* **2013**, *42*, 14498–14508. [[CrossRef](#)] [[PubMed](#)]
12. Papes Filho, A.C.; Maciel Filho, R. Hybrid training approach for artificial neural networks using genetic algorithms for rate of reaction estimation: Application to industrial methanol oxidation to formaldehyde on silver catalyst. *Chem. Eng. J.* **2010**, *157*, 501–508. [[CrossRef](#)]
13. Slot Thierry, K.; Eisenberg, D.; van Noordenne, D.; Jungbacker, P.; Rothenberg, G. Cooperative catalysis for selective alcohol oxidation with molecular oxygen. *Chem. Eur. J.* **2016**, *22*, 12307–12311. [[CrossRef](#)] [[PubMed](#)]
14. Vinod, C.P.; Wilson, K.; Lee Adam, F. Recent advances in the heterogeneously catalysed aerobic selective oxidation of alcohols. *J. Chem. Technol. Biotechnol.* **2011**, *86*, 161–171. [[CrossRef](#)]
15. Kopylovich, M.N.; Ribeiro, A.P.C.; Alegria, E.C.B.A.; Martins, N.M.R.; Martins, L.M.D.R.S.; Pombeiro, A.J.L. Chapter Three-Catalytic oxidation of alcohols: Recent advances. In *Advances in Organometallic Chemistry*; Pérez, P.J., Ed.; Academic Press: Cambridge, MA, USA, 2015; Volume 63, pp. 91–174.
16. Enache, D.I.; Edwards, J.K.; Landon, P.; Solsona-Espriu, B.; Carley, A.F.; Herzing, A.A.; Watanabe, M.; Kiely, C.J.; Knight, D.W.; Hutchings, G.J. Solvent-free oxidation of primary alcohols to aldehydes using Au-Pd/TiO<sub>2</sub> catalysts. *Science* **2006**, *311*, 362–365. [[CrossRef](#)] [[PubMed](#)]
17. Sharma, A.S.; Kaur, H.; Shah, D. Selective oxidation of alcohols by supported gold nanoparticles: Recent advances. *RSC Adv.* **2016**, *6*, 28688–28727. [[CrossRef](#)]
18. Mallat, T.; Baiker, A. Oxidation of alcohols with molecular oxygen on platinum metal catalysts in aqueous solutions. *Catal. Today* **1994**, *19*, 247–283. [[CrossRef](#)]
19. Wang, H.; An, K.; Sapi, A.; Liu, F.; Somorjai, G.A. Effects of nanoparticle size and metal/support interactions in pt-catalyzed methanol oxidation reactions in gas and liquid phases. *Catal. Lett.* **2014**, *144*, 1930–1938. [[CrossRef](#)]
20. Sapi, A.; Liu, F.; Cai, X.; Thompson, C.M.; Wang, H.; An, K.; Krier, J.M.; Somorjai, G.A. Comparing the catalytic oxidation of ethanol at the solid–gas and solid–liquid interfaces over size-controlled pt nanoparticles: Striking differences in kinetics and mechanism. *Nano Lett.* **2014**, *14*, 6727–6730. [[CrossRef](#)] [[PubMed](#)]

21. Liu, F.; Han, H.-L.; Carl, L.M.; Zherebetsky, D.; An, K.; Wang, L.-W.; Somorjai, G.A. Catalytic 1-propanol oxidation on size-controlled platinum nanoparticles at solid-gas and solid-liquid interfaces: Significant differences in kinetics and mechanisms. *J. Phys. Chem. C* **2018**. [CrossRef]
22. Wang, H.; Sapi, A.; Thompson, C.M.; Liu, F.; Zherebetsky, D.; Krier, J.M.; Carl, L.M.; Cai, X.; Wang, L.-W.; Somorjai, G.A. Dramatically different kinetics and mechanism at solid/liquid and solid/gas interfaces for catalytic isopropanol oxidation over size-controlled platinum nanoparticles. *J. Am. Chem. Soc.* **2014**, *136*, 10515–10520. [CrossRef] [PubMed]
23. Saturated Vapor Pressure. Available online: <http://ddbonline.ddbst.com/AntoineCalculation/AntoineCalculationCGI.exe> (accessed on 1 February 2018).
24. NIST Chemistry WebBook. Available online: <https://webbook.nist.gov/cgi/inchi?ID=C71238&Mask=4&Type=ANTOINE&Plot=on> (accessed on 1 February 2018).
25. Kemme, H.R.; Kreps, S.I. Vapor pressure of primary n-alkyl chlorides and alcohols. *J. Chem. Eng. Data* **1969**, *14*, 98–102. [CrossRef]
26. Kobayashi, H.; Higashimoto, S. DFT study on the reaction mechanisms behind the catalytic oxidation of benzyl alcohol into benzaldehyde by O<sub>2</sub> over anatase TiO<sub>2</sub> surfaces with hydroxyl groups: Role of visible-light irradiation. *Appl. Catal. B Environ.* **2015**, *170–171*, 135–143. [CrossRef]
27. Welty, J.R.; Wicks, C.E.; Wilson, R.E.; Rorrer, G.L. *Fundamentals of Momentum, Heat, and Mass Transfer 5th Edition*; John Wiley & Sons, Inc.: New York, NY, USA, 2007; ISBN 2900470128687.
28. Ferrell, R.T.; Himmelblau, D.M. Diffusion coefficients of nitrogen and oxygen in water. *J. Chem. Eng. Data* **1967**, *12*, 111–115. [CrossRef]
29. Alger, D.B. The water solubility of 2-butanol: A widespread error. *J. Chem. Educ.* **1991**, *68*, 939. [CrossRef]
30. Mullen, G.M.; Zhang, L.; Evans, E.J.; Yan, T.; Henkelman, G.; Mullins, C.B. Oxygen and hydroxyl species induce multiple reaction pathways for the partial oxidation of allyl alcohol on gold. *J. Am. Chem. Soc.* **2014**, *136*, 6489–6498. [CrossRef] [PubMed]
31. Mullen, G.M.; Zhang, L.; Evans, E.J.; Yan, T.; Henkelman, G.; Mullins, C.B. Control of selectivity in allylic alcohol oxidation on gold surfaces: The role of oxygen adatoms and hydroxyl species. *Phys. Chem. Chem. Phys.* **2015**, *17*, 4730–4738. [CrossRef] [PubMed]
32. Thompson, C.M.; Carl, L.M.; Somorjai, G.A. Sum frequency generation study of the interfacial layer in liquid-phase heterogeneously catalyzed oxidation of 2-propanol on platinum: Effect of the concentrations of water and 2-propanol at the interface. *J. Phys. Chem. C* **2013**, *117*, 26077–26083. [CrossRef]
33. Kresse, G.; Furthmüller, J. Efficient iterative schemes for ab initio total-energy calculations using a plane-wave basis set. *Phys. Rev. B* **1996**, *54*, 11169–11186. [CrossRef]
34. Kresse, G.; Joubert, D. From ultrasoft pseudopotentials to the projector augmented-wave method. *Phys. Rev. B* **1999**, *59*, 1758–1775. [CrossRef]
35. Klimeš, J.; Bowler, D.R.; Michaelides, A. Van der waals density functionals applied to solids. *Phys. Rev. B* **2011**, *83*, 195131. [CrossRef]
36. Román-Pérez, G.; Soler, J.M. Efficient implementation of a van der waals density functional: Application to double-wall carbon nanotubes. *Phys. Rev. Lett.* **2009**, *103*, 096102. [CrossRef] [PubMed]
37. Perdew, J.P.; Chevary, J.A.; Vosko, S.H.; Jackson, K.A.; Pederson, M.R.; Singh, D.J.; Fiolhais, C. Atoms, molecules, solids, and surfaces: Applications of the generalized gradient approximation for exchange and correlation. *Phys. Rev. B* **1992**, *46*, 6671–6687. [CrossRef]

